

Received May 29, 2020, accepted June 29, 2020, date of publication July 6, 2020, date of current version July 16, 2020.

Digital Object Identifier 10.1109/ACCESS.2020.3007216

Methods of Controlling Lift-Off in Conductivity Invariance Phenomenon for Eddy Current Testing

ZHONGWEN JIN¹, YUWEI MENG¹, RONGDONG YU¹, RUOCHEN HUANG^{1,2},
MINGYANG LU², (Member, IEEE), HANYANG XU², XIAOBAI MENG³, QIAN ZHAO⁴,
ZHIJIE ZHANG⁵, ANTHONY PEYTON², AND WULIANG YIN², (Senior Member, IEEE)

¹Zhejiang Energy Group Research Institute, Hangzhou 311121, China

²School of Electrical and Electronics Engineering, The University of Manchester, Manchester M13 9PL, U.K.

³Faculty of Arts, Science, and Technology, The University of Northampton, Northampton NN2 6JD, U.K.

⁴College of Engineering, Qufu Normal University, Shandong 273165, China

⁵School of Instrument and Electronics, North University of China, Taiyuan 030051, China

Corresponding authors: Ruochen Huang (ruochen.huang@manchester.ac.uk) and Mingyang Lu (mingyang.lu@manchester.ac.uk)

This work was supported by the U.K. Engineering and Physical Sciences Research Council (EPSRC) under Grant EP/P027237/1 [real-time in-line microstructural engineering (RIME)].


ABSTRACT Previously, a conductivity invariance phenomena (CIP) has been discovered – at a certain lift-off, the inductance change of the sensor due to a test sample is immune to conductivity variations, i.e. the inductance – lift-off curve passes through a common point at a certain lift-off, termed as conductivity invariance lift-off. However, this conductivity invariance lift-off is fixed for a particular sensor setup, which is not convenient for various sample conditions. In this paper, we propose using two parameters in the coil design – the horizontal and vertical distances between the transmitter and the receiver to control the conductivity invariance lift-off. The relationship between these two parameters and the conductivity invariance lift-off is investigated by simulation and experiments and it has been found that there is an approximate linear relationship between these two parameters and the conductivity invariance lift-off. This is useful for applications where the measurements have restrictions on lift-off, e.g. uneven coating thickness which limits the range of the lift-off of probe during the measurements. Therefore, based on this relationship, it can be easier to adjust the configuration of the probe for a better inspection of the test samples.

INDEX TERMS Conductivity invariance phenomenon, conductivity invariance lift-off, sensor design, Eddy current testing, electrical conductivity, non-destructive testing.

I. INTRODUCTION

In recent decades, non-destructive testing (NDT) has been widely used. Eddy current testing (ECT), as one of the most universal NDT techniques, has extensive applications for thickness measurement, the inspection of material integrity (e.g. crack detection) and the evaluation of material properties (e.g. electrical conductivity and magnetic permeability) [1]–[7]. However, the testing is significantly influenced by the material properties, lift-off and sensor structure, etc. As a result, various researches have been carried out to tackle this issue in pursuit of a better inspection of the test sample [8]–[16].

A precise estimation of the electrical conductivity and the magnetic permeability of the test sample is essential in

The associate editor coordinating the review of this manuscript and approving it for publication was Michele Magno .

many applications. Halleux *et al.* developed an equivalent simplified physical model for the electrical conductivity measurement and it can be applied in a wide range of metallic samples [17]. Moreover, a robust method by using frequency-dependent eddy current measurements was presented by Moulder *et al.* to determine the electrical conductivity of the uniform conductive layers [18]. Conductivity profiling from inductance spectroscopic measurements [19] and the conductivity measuring instrument for semi-conductors [20] also have been explored.

In terms of permeability measurements, it is still challenging to determine the permeability of the material due to the influence of the environment condition and the material conductivity on the response signal. A novel method that can measure the conductivity and permeability of the metal samples simultaneously was proposed by Ma *et al.* [21]. The conductivity can be obtained by the impedance change

of the signal while the permeability can be measured by utilising the imaginary part of the signal. The results were proved to be accurate but the frequency range is limited for estimating permeability. Yu *et al.* proposed the CIP and developed a device to determine the permeability by decoupling the influence of the conductivity and permeability [22], [23]. Besides, a novel algorithm to compensate for the zero-crossing frequency point caused by the lift-off effect was proposed by Lu *et al.* and the error caused by the lift-off can be reduced to 7.5% [24], [25]. Moreover, for the thick coating, the lift-off effect in PEC can be reduced by using the reference signals and normalization process [26] and it is found that the sensitivity of the sensor coil would be boosted with higher lift-off under a certain range of the coil gap [27].

In our previous work, measurement of permeability for ferrite metallic plates based on CIP was introduced and proved to work well [28]. Further, in this paper, we proposed using two parameters in the coil design – the horizontal and vertical distances between the transmitter and the receiver to control the conductivity invariance lift-off to make it more flexible in ECT where the measurements have restrictions on lift-off, e.g. uneven coating thickness and varying coating thickness which limit the range of the lift-off of the probe during the measurements.

II. SENSOR PARAMETERS FOR CONTROLLING CIP LIFT-OFF

In order to investigate the conductivity invariance phenomenon, the arrangement of the excitation coil and the receiving coil should be non-axial to the test samples (showed in Fig. 1), otherwise, there is no conductivity invariance lift-off point from measurements.

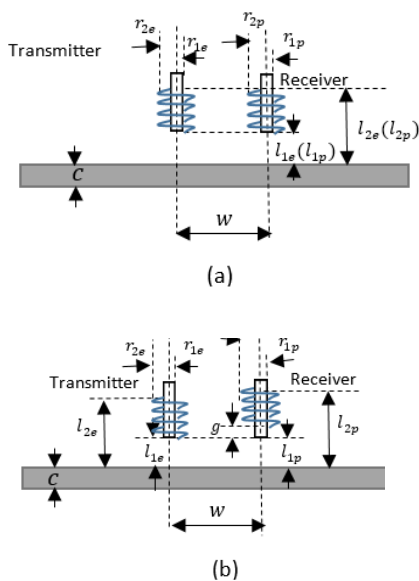


FIGURE 1. Sensor geometry (a) Sensor A, transmitter and receiver are assembled in the same plane (b) sensor B, receiver is vertically lifted with respect to the transmitter.

For a particular non-axial sensor setup, the lift-off point of CIP is fixed. In this paper, we introduce two parameters, that is, the horizontal distance (w) and vertical distance (g) between the transmitter and the receiver to control the CIP lift-off. Two sensor setups are used for the investigation of how these two parameters affect the CIP lift-off, named as, Sensor A and Sensor B. Fig. 1 (a) depicts the configuration where the transmitter and receiver are placed in the same vertical level, while Fig. 1 (b) presents the case where the receiver is vertically lifted by a distance of g . By adjusting the value of these two parameters, the value of the lift-off of CIP would change accordingly. Hence, it is more beneficial for the permeability measurement that has a limited range of lift-off.

III. ANALYTICAL SOLUTION ON CIP LIFT-OFF

The complex inductance of an air-cored cylindrical coil caused by the metallic plate has been proposed by Dodd and Deeds for decades to offer strong interpretations of the electromagnetic phenomenon. Based on the formula of Dodd and Deeds analytical solution, the vector potentials from the excitation coil caused by the sample plate can be expressed as,

$$\begin{aligned}
 A(r, z) &= \frac{\mu_0 I N_1}{(r_{2e} - r_{1e})(l_{2e} - l_{1e})} \int_0^\infty \frac{1}{\alpha^3} I(r_{2e}, r_{1e}) J_1(\alpha r) \\
 &\times [2 - e^{\alpha(z-l_{2e})} - e^{\alpha(z-l_{1e})} + e^{-\alpha z} (e^{-\alpha l_{1e}} - e^{-\alpha l_{2e}})] \\
 &\times \frac{(\alpha_1 + \mu\alpha)(\alpha_1 - \mu\alpha) - (\alpha_1 + \mu\alpha)(\alpha_1 - \mu\alpha) e^{2\alpha_1 c}}{- (\alpha_1 - \mu\alpha)(\alpha_1 - \mu\alpha) + (\alpha_1 + \mu\alpha)(\alpha_1 + \mu\alpha) e^{2\alpha_1 c}} \frac{1}{\alpha} d\alpha
 \end{aligned} \tag{1}$$

$$\alpha_1 = \sqrt{\alpha^2 + j\omega\sigma\mu\mu_0} \tag{2}$$

where: μ_0 denotes the permeability of the free space, σ and μ denote the electrical conductivity and permeability of the sample plate, α denotes the spatial frequency variable, I denotes the excitation current flows in the coil, N_1 denotes the number of turns of the excitation coil, r_{1e} and r_{2e} denote the inner radius and the outer radius of the excitation coil, l_{1e} and l_{2e} denote the bottom height and top height of the excitation coil, $J_1(x)$ denotes the first order of the first kind of Bessel function and $I(x_1, x_2)$ denotes the production of, $J_1(x)$ from x_1 to x_2 .

Furthermore, the voltage induced by a single loop of the receiving coil (Fig. 2) can be expressed as an integration of the vector potential over the cross-section of the coil.

$$V = j\omega \int A(r, z) ds = j\omega \int A(r, z) r_p \cos\varphi d\theta \tag{3}$$

$$\varphi = \theta + \tan^{-1} \left(\frac{r_p \sin\theta}{w - r_p \cos\theta} \right) \tag{4}$$

$$r = \sqrt{(r_p \sin\theta)^2 + (w - r_p \cos\theta)^2 + g^2} \tag{5}$$

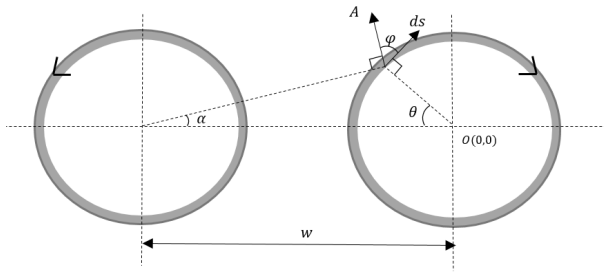


FIGURE 2. Top view of sensor coils.

where: φ denotes the angle between the vector potential A and ds , r denotes the distance between the origin O and ds , g denotes the height difference between the excitation coil and receiving coil.

The voltage received in the receiving coil can be derived by combining (1)-(5). Two situations of sensor arrangement are considered, as shown in Fig. 1 (a) and (b). Hence the voltage induced can be expressed as (6) for Fig. 1(a) and (7) for Fig. 1(b).

$$\begin{aligned}
 V_a &= \frac{jw\mu_0IN_1N_2}{(r_{2e} - r_{1e})(l_{2e} - l_{1e})(r_{2p} - r_{1p})(l_{2p} - l_{1p})} \\
 &\times \int_0^\infty \int_0^{2\pi} \int_{r_{1p}}^{r_{2p}} \cos\left(\theta + \tan^{-1}\left(\frac{r_p \sin\theta}{w - r_p \cos\theta}\right)\right) \\
 &\times \frac{1}{\alpha^3} I(r_{2e}, r_{1e}) J\left(\alpha \sqrt{(r_p \sin\theta)^2 + (w - r_p \cos\theta)^2}\right) \\
 &\times \left(2(l_{2e} - l_{1e}) - \frac{1}{\alpha} [2e^{-\alpha(l_{2e} - l_{1e})} - 2\right. \\
 &\left. + (e^{-\alpha l_{1e}} - e^{-\alpha l_{2e}})^2\right) \\
 &\times \frac{(\alpha_1 + \mu\alpha)(\alpha_1 - \mu\alpha) - (\alpha_1 + \mu\alpha)(\alpha_1 - \mu\alpha)e^{2\alpha_1 c}}{-\alpha_1 - \mu\alpha)(\alpha_1 - \mu\alpha) + (\alpha_1 + \mu\alpha)(\alpha_1 + \mu\alpha)e^{2\alpha_1 c}} \\
 &\times dr_p d\theta d\alpha \quad (6)
 \end{aligned}$$

$$\begin{aligned}
 V_b &= \frac{jw\mu_0IN_1N_2}{(r_{2e} - r_{1e})(l_{2e} - l_{1e})(r_{2p} - r_{1p})(l_{2p} - l_{1p})} \\
 &\times \int_0^\infty \int_0^{2\pi} \int_{r_{1p}}^{r_{2p}} \cos\left(\theta + \tan^{-1}\left(\frac{r_p \sin\theta}{w - r_p \cos\theta}\right)\right) \\
 &\times \frac{1}{\alpha^3} I(r_{2e}, r_{1e}) J\left(\alpha \sqrt{(r_p \sin\theta)^2 + (w - r_p \cos\theta)^2 + g^2}\right) \\
 &\times \left(2(l_{2p} - l_{1p}) - \frac{1}{\alpha} [e^{-\alpha(l_{2p} - l_{2e})} - e^{-\alpha(l_{1p} - l_{2e})}\right. \\
 &\left. + e^{-\alpha(l_{2p} - l_{1e})} - e^{-\alpha(l_{1p} - l_{1e})} + (e^{-\alpha l_{2p}} - e^{-\alpha l_{1p}})\right) \\
 &\times (e^{-\alpha l_{1e}} - e^{-\alpha l_{2e}}) \\
 &\times \frac{(\alpha_1 + \mu\alpha)(\alpha_1 - \mu\alpha) - (\alpha_1 + \mu\alpha)(\alpha_1 - \mu\alpha)e^{2\alpha_1 c}}{-\alpha_1 - \mu\alpha)(\alpha_1 - \mu\alpha) + (\alpha_1 + \mu\alpha)(\alpha_1 + \mu\alpha)e^{2\alpha_1 c}} \\
 &\times dr_p d\theta d\alpha \quad (7)
 \end{aligned}$$

where: N_2 denotes the number of turns of the sensing coil, r_{1p} and r_{2p} denote the inner radius and the outer radius of the sensing coil, l_{1p} and l_{2p} denote the bottom height and top height of the sensing coil.

With further manipulations from (6) and (7), the complex mutual inductance between the excitation coil and the receiving coil can be derived as (8) for Fig. 1(a) and (9) for Fig. 1(b).

$$\begin{aligned}
 L_a &= \frac{\mu_0 N_1 N_2}{(r_{2e} - r_{1e})(l_{2e} - l_{1e})(r_{2p} - r_{1p})(l_{2p} - l_{1p})} \\
 &\times \int_0^\infty \int_0^{2\pi} \int_{r_{1p}}^{r_{2p}} \cos\left(\theta + \tan^{-1}\left(\frac{r_p \sin\theta}{w - r_p \cos\theta}\right)\right) \\
 &\times \frac{1}{\alpha^3} I(r_{2e}, r_{1e}) J\left(\alpha \sqrt{(r_p \sin\theta)^2 + (w - r_p \cos\theta)^2}\right) \\
 &\times \left(2(l_{2e} - l_{1e}) - \frac{1}{\alpha} [2e^{-\alpha(l_{2e} - l_{1e})} - 2\right. \\
 &\left. + (e^{-\alpha l_{1e}} - e^{-\alpha l_{2e}})^2\right) \\
 &\times \frac{(\alpha_1 + \mu\alpha)(\alpha_1 - \mu\alpha) - (\alpha_1 + \mu\alpha)(\alpha_1 - \mu\alpha)e^{2\alpha_1 c}}{-\alpha_1 - \mu\alpha)(\alpha_1 - \mu\alpha) + (\alpha_1 + \mu\alpha)(\alpha_1 + \mu\alpha)e^{2\alpha_1 c}} \\
 &\times dr_p d\theta d\alpha \quad (8)
 \end{aligned}$$

$$\begin{aligned}
 L_b &= \frac{\mu_0 N_1 N_2}{(r_{2e} - r_{1e})(l_{2e} - l_{1e})(r_{2p} - r_{1p})(l_{2p} - l_{1p})} \\
 &\times \int_0^\infty \int_0^{2\pi} \int_{r_{1p}}^{r_{2p}} \cos\left(\theta + \tan^{-1}\left(\frac{r_p \sin\theta}{w - r_p \cos\theta}\right)\right) \\
 &\times \frac{1}{\alpha^3} I(r_{2e}, r_{1e}) J\left(\alpha \sqrt{(r_p \sin\theta)^2 + (w - r_p \cos\theta)^2 + g^2}\right) \\
 &\times \left(2(l_{2p} - l_{1p}) - \frac{1}{\alpha} [e^{-\alpha(l_{2p} - l_{2e})} - e^{-\alpha(l_{1p} - l_{2e})}\right. \\
 &\left. + e^{-\alpha(l_{2p} - l_{1e})} - e^{-\alpha(l_{1p} - l_{1e})} + (e^{-\alpha l_{2p}} - e^{-\alpha l_{1p}})\right) \\
 &\times (e^{-\alpha l_{1e}} - e^{-\alpha l_{2e}}) \\
 &\times \frac{(\alpha_1 + \mu\alpha)(\alpha_1 - \mu\alpha) - (\alpha_1 + \mu\alpha)(\alpha_1 - \mu\alpha)e^{2\alpha_1 c}}{-\alpha_1 - \mu\alpha)(\alpha_1 - \mu\alpha) + (\alpha_1 + \mu\alpha)(\alpha_1 + \mu\alpha)e^{2\alpha_1 c}} \\
 &\times dr_p d\theta d\alpha \quad (9)
 \end{aligned}$$

Here, all the analytical solutions were calculated via the platform ThinkCenter M910s, with 16GB RAM and Intel Core i7-6700 processor.

IV. EXPERIMENTAL SETUP ON CIP LIFT-OFF

Due to the restriction in access such as coating thickness on the test sample, there exists a minimum lift-off during inspection. To address this issue, both simulation by analytical calculation and the experimental measurements have been carried out to verify the relationship between the horizontal and vertical distances of the sensor coils and the conductivity invariance lift-off point.

During the experimental measurements, the sensor shown in Fig. 3 was used to detect the feature of this phenomenon. The horizontal distance between two sensor coils was set to 3 mm, 4 mm and 5 mm respectively. The test samples have a length of 80 mm, a width of 80 mm and a

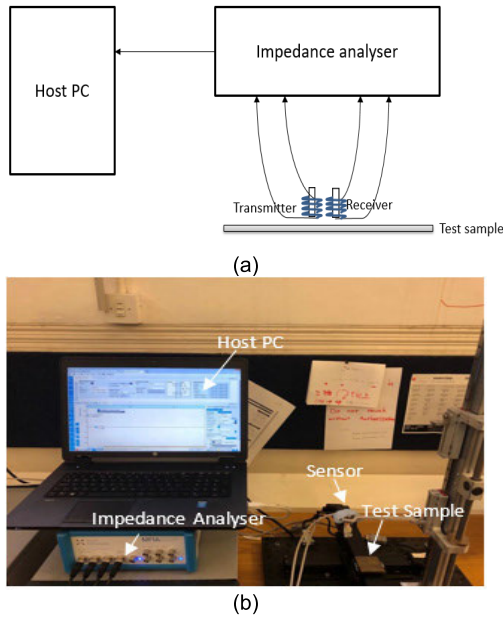


FIGURE 3. Experimental setup (a) schematic setup (b) actual setup.

TABLE 1. Sensor parameters.

Inner and outer radii of the excitation coil (r_{1e} / r_{2e})	0.75 mm/0.95 mm
Inner and outer radii of the receiving coil (r_{1p} / r_{2p})	0.75 mm/1.10 mm
Height of the excitation coil ($l_{2e} - l_{1e}$)	3 mm
Height of the receiving coil ($l_{2p} - l_{1p}$)	3 mm
Turns of excitation coil and receiving coil (N_1 / N_2)	120/160
Plate thickness (c)	5 mm
The horizontal distance between two coils (w)	3 – 5 mm
The vertical distance between two coils	-1 – 1 mm

thickness of 5 mm. Three types of materials were tested under the excitation frequency of 60 kHz, copper, aluminium and brass respectively. The conductivities of these materials are 57 MS/m, 35 MS/m, 16 MS/m at 20 degrees and the relative permeability is 1 for conductive materials. The experimental setup is showed in Fig. 3 and the sensor parameters are listed in Table 1.

From the schematic setup shown in Fig. 3(a), the injection current flows into the transmitter and can induce the voltage on the receiver, then the impedance between the transmitter and the receiver can be obtained via the impedance analyser. It is because there is a phase difference between the induced voltage and the excitation current, the tested impedance should be complex. Therefore, the complex inductance can be presented by dividing the mutual impedance by the excitation frequency in the experimental measurements, as shown in (10)-(13). Further, the inductance of one of the metal plates was set as a reference for the inductance of all the samples, the conductivity invariance lift-off can be found by the

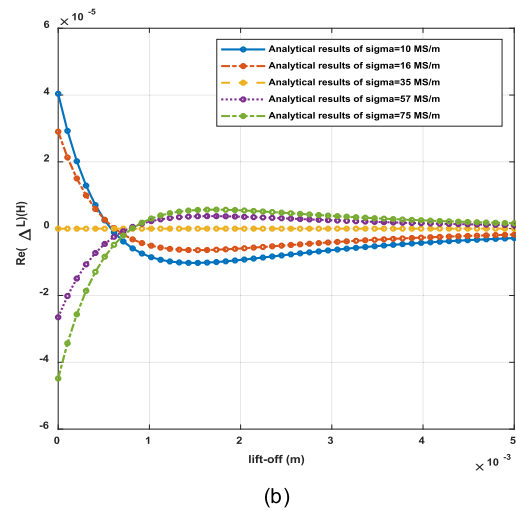
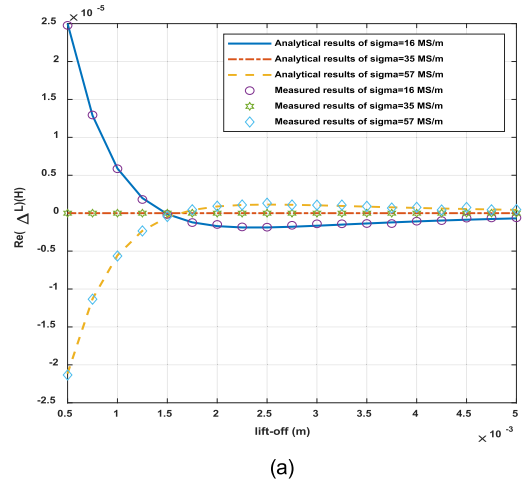


FIGURE 4. CIP validation (a) results of conductive materials ($\mu_r = 1$) (b) analytical solution of ferromagnetic materials under ($\mu_r = 300$).

inductance changes with respect to the reference inductance. It is worth noting that the real part of the inductance change is mainly due to the change of the magnetic flux affected by the metallic plate, meanwhile, the loss mainly due to the eddy current effect reflects on the change of the imaginary part of the inductance.

$$Z = R + j\omega L \tag{10}$$

$$\Delta L = \frac{\Delta Z}{j\omega} \tag{11}$$

$$\text{Re}(\Delta L) = \text{Re}\left(\frac{Z_{\text{sample}} - Z_{\text{air}}}{j\omega}\right) \tag{12}$$

$$\text{Im}(\Delta L) = \text{Im}\left(\frac{Z_{\text{sample}} - Z_{\text{air}}}{j\omega}\right) \tag{13}$$

where: Z_{sample} denotes the impedance caused by the metallic sample plate and Z_{air} denotes the impedance in the air.

V. RESULTS

A. VALIDATION OF CIP LIFT-OFF

Through experimental results and simulation results shown in Fig. 4, there exists the conductivity invariance lift-off

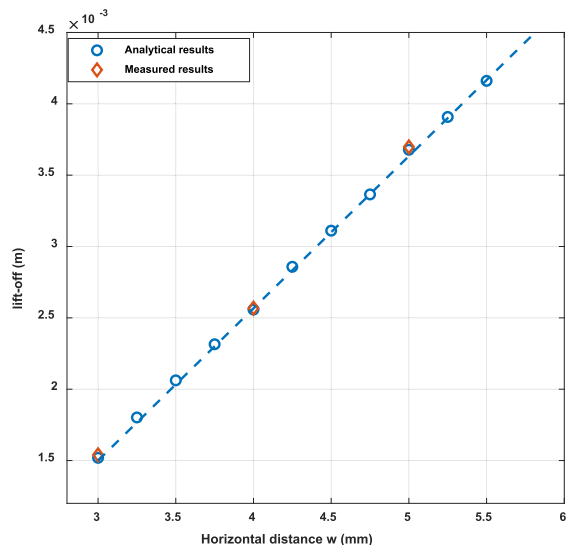


FIGURE 5. The analytical and measured results of the conductivity invariance lift-off under different horizontal distances between the sensor coils from sensor A.

for the non-magnetic conductive / ferromagnetic materials. The maximum error between the experiments and simulations for varying lift-off is 7.46% for Fig. 4 (a). However, at the conductivity invariance lift-off point, the error of the inductance variation can be neglected since it is controlled within a relatively small range of 0.1%. Therefore, it is an ideal sensor position for material inspection under different configurations of the sensor. For permeability measurements with the material in which the conductivities are known, assume all the materials with the same permeability, the conductivity invariance lift-off can be obtained from the simulation, as shown in Fig. 4(b). Compared with the results from Fig. 4(a), the conductivity invariance lift-off decreases as the relative permeability increases. Thus, from the experimental measurements under this conductivity invariance lift-off, the permeability can be predicted from the offset of the curves.

B. CIP LIFT-OFF EVALUATION

To investigate the relationship between the horizontal/vertical distance of the transmitter and the receiver and the CIP, both the analytical simulations and experiments have been carried out. A linear relationship has been found between the horizontal/vertical distance of the transmitter and the receiver and the CIP, as shown in the following Fig. 5 and 6.

1) HORIZONTAL DISTANCE

In this section, sensor A (showed in Fig. 1(a)) was used to investigate how the relationship between the horizontal distance and the conductivity invariance lift-off changes. Table 2 illustrates the error between the simulated results and the measured results. The error between them can be achieved within 1.5%. More horizontal distances (in steps of 0.25 mm) have been considered by utilizing the analytical solution and

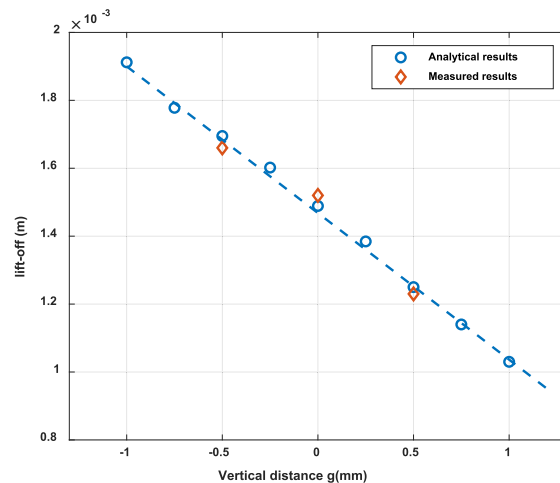


FIGURE 6. The analytical results of the conductivity invariance lift-off point under different vertical distances and fixed horizontal distance w of 3 mm.

TABLE 2. Simulated and measured conductivity invariance lift-off points under different horizontal distance.

Horizontal distance between two sensor coils (w)	Simulated conductivity invariance lift-off (m)	Measured conductivity invariance lift-off (m)	Error (%)
3 mm	1.51e-3	1.53e-3	1.32
4 mm	2.56e-3	2.57e-3	0.39
5 mm	3.67e-3	3.70e-3	0.82

the results are shown in Fig. 5. The dashed line shows the trend of the change of conductivity invariance lift-off. As the horizontal distance increases, the lift-off increases to observe the predominant magnetic flux passing through the receiver regardless of the sample conductivities. It can be noticed that there is an approximated linear relationship between the horizontal distance of sensor coils and the conductivity invariance lift-off.

2) VERTICAL DISTANCE

As shown in Fig. 1(b), sensor B was used to investigate how the conductivity invariance lift-off changes with the vertical distance. For experimental measurements, the vertical distance between the excitation coil and the sensing coil was set to -0.5 mm (the receiver is 0.5 mm lower than the transmitter), 0 mm, and 0.5 mm (the receiver is 0.5 mm higher than the transmitter) respectively while the horizontal distance was kept to 3 mm. The analytical solution was used to simulate more possible vertical distance to evaluate the relations (the vertical distance changes from -1 mm to 1 mm in steps of 0.25 mm). The results are presented in Fig. 6. The trends of the results are matched with the trend lines (dashed lines). Table 3 depicts the conductivity invariance lift-off between simulation and measurements and the error is within 3%. It can be seen from Fig. 6 that there is a decreasing trend as

TABLE 3. Simulated and measured conductivity invariance lift-off points under different vertical distance.

Vertical distance between two sensor coils (g)	Simulated conductivity invariance lift-off (m)	Measured conductivity invariance lift-off (m)	Error (%)
-0.5 mm	1.69e-3	1.66e-3	-1.78
0 mm	1.49e-3	1.53e-3	2.68
0.5 mm	1.25e-3	1.23e-3	-1.60

the receiver move from the bottom up with respect to the transmitter. Thus, there is a trade-off for researchers to select the configurations for the sensor through these relations to match their measurement conditions.

VI. DISCUSSIONS

A. EFFECT OF SAMPLE THICKNESS

The thickness of the samples has an influence on the conductivity invariance lift-off. In the numerical simulation, sensor A was used and the sample thicknesses are 0.05 mm, 1 mm, 5 mm and 15 mm respectively. All the samples were simulated under the excitation frequency of 60 kHz. The conductivities of the samples were set to 16 MS/m, 35 MS/m and 57 MS/m respectively with the relative permeability of 1. Conductivity invariance lift-off for different sample thicknesses goes along with the dashed lines showed in Fig. 8. It is found that there is no conductivity invariance lift-off as the sample thickness was 0.05 mm (Fig. 7) while the conductivity invariance lift-off does not increase any more as the sample thickness reaches a certain amount (Fig. 8). The reason that there is no conductivity invariance lift-off is that the skin depth is larger than the thickness of the samples so that most of the magnetic flux penetrates through the samples, which could influence the vector potential to be integrated on the cross-section of the sensing coil (i.e. the induced voltage) as the sensor moving vertically. As the sample thickness increases to a certain range, the skin depth is smaller than the sample thickness, all the magnetic flux would be reflected by the test samples and the induced voltage on the sensor coil. Therefore, the conductivity invariance lift-off stays at a similar value. It can be seen in Fig. 8 that the conductivity invariance lift-off decreases as the sample becomes thicker while for the arbitrary thickness of the test samples, there is a linear trend between the conductivity invariance lift-off and the horizontal distance of the sensor coils.

B. EFFECT OF DIFFERENT FREQUENCIES

Fig. 9 demonstrates the simulation results of the conductivity invariance lift-off under two excitation frequencies: 50 kHz and 500 kHz. During the simulation, the thickness of the test samples is set to be 1 mm and sensor A was used. As shown in Fig. 9, with a fixed sensor setup, a higher excitation frequency will lead to an increase of the conductivity invariance lift-off, which is due to the skin depth effect. For different frequencies, the lift-off increases linearly with the increase of the

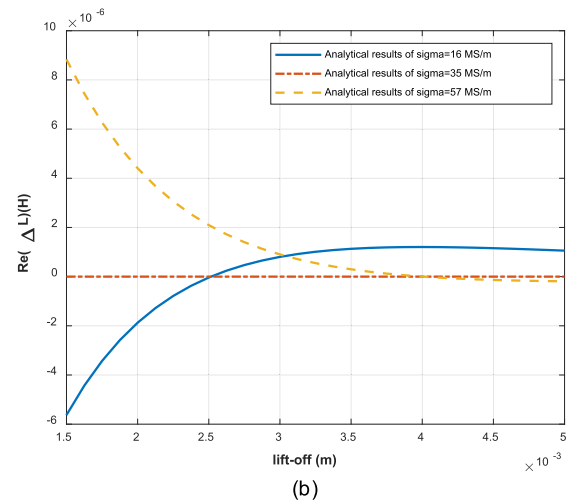
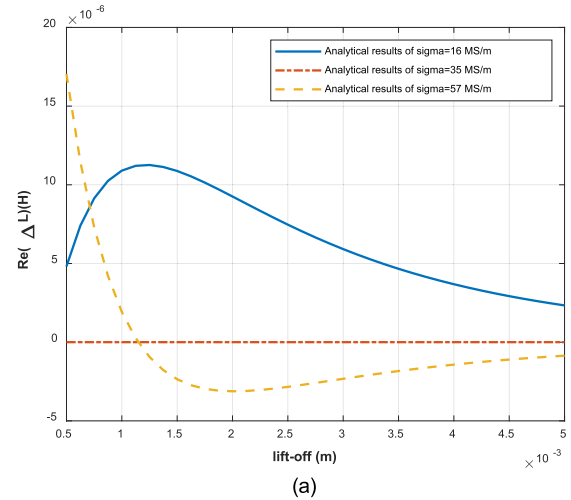


FIGURE 7. Analytical solution of the sample thickness 0.05 mm under different widths between the sensor coils (a) 3 mm (b) 5 mm.

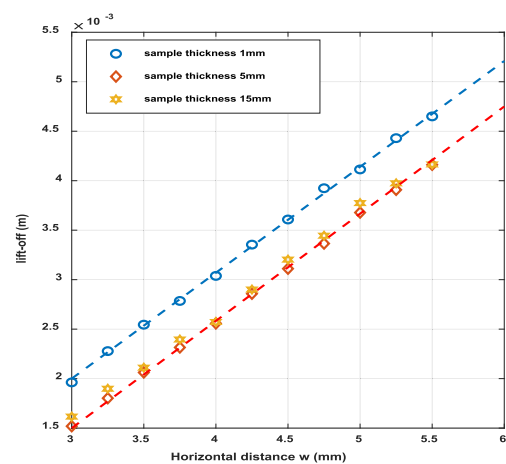


FIGURE 8. Conductivity invariance lift-off under different horizontal distances between the sensor coils and sample thicknesses.

width, as shown by the dashed line (trend line). Additionally, it can be noticed that, as the horizontal distance between two coils gradually increases, the difference of the lift-off between

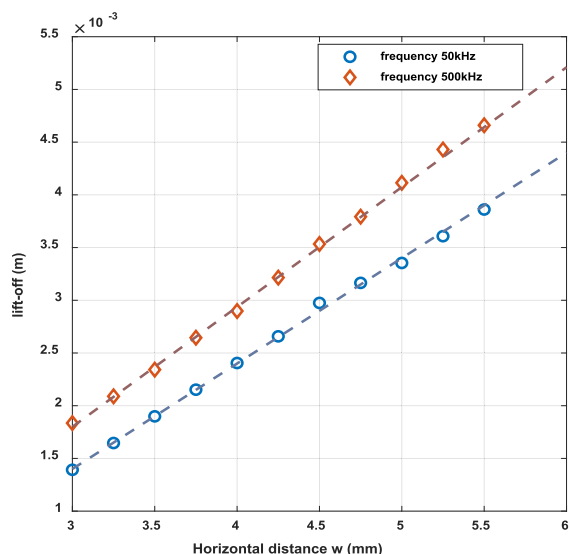


FIGURE 9. Analytical solutions of conductivity invariance lift-off under different horizontal distances between the sensor coils and excitation frequencies.

the results under the frequency of 500 kHz and 50 kHz is slightly larger.

VII. CONCLUSIONS

The conductivity invariance lift-off exists when the arrangement of the excitation coil and the receiving coil is non-axial to the sample plates. In this paper, the impact of changing horizontal and vertical distance between the transmitter coil and the receiver coil on the conductivity invariance lift-off was investigated. It is found that there is a good linear relationship between them for materials of different electrical conductivities. Both the analytical and measured results have verified this relationship.

Based on this feature, the conductivity invariance lift-off can be adjusted for cases where there is restriction of access to the test sample. Moreover, the effect of the sample thickness and the excitation frequency on the relations are all discussed, and it proves that linear relation is always valid for these factors.

REFERENCES

- [1] G. Y. Tian, A. Sophian, D. Taylor, and J. Rudlin, "Multiple sensors on pulsed eddy-current detection for 3-D subsurface crack assessment," *IEEE Sensors J.*, vol. 5, no. 1, pp. 90–96, Feb. 2005.
- [2] C. Ye, Y. Huang, L. Udpa, S. Udpa, and A. Tamburrino, "Magnetoresistive sensor with magnetic balance measurement for inspection of defects under magnetically permeable fasteners," *IEEE Sensors J.*, vol. 16, no. 8, pp. 2331–2338, Apr. 2016.
- [3] J. R. Salas Avila, K. Y. How, M. Lu, and W. Yin, "A novel dual modality sensor with sensitivities to permittivity, conductivity, and permeability," *IEEE Sensors J.*, vol. 18, no. 1, pp. 356–362, Jan. 2018.
- [4] W. Yin, A. J. Peyton, and S. J. Dickinson, "Simultaneous measurement of distance and thickness of a thin metal plate with an electromagnetic sensor using a simplified model," *IEEE Trans. Instrum. Meas.*, vol. 53, no. 4, pp. 1335–1338, Aug. 2004.
- [5] X. Ma, A. J. Peyton, and Y. Zhao, "Measurement of the electrical conductivity of open-celled aluminium foam using non-contact eddy current techniques," *NDT E Int.*, vol. 38, pp. 359–397, Jul. 2005.
- [6] B. Ye, J. Cai, P. Huang, M. Fan, and Z. Zhou, "Automatic recognition and classification of eddy current testing signals for scanning inspection of defect in multi-layered structures," *Chin. J. Sens. Actuators*, vol. 20, no. 10, pp. 2253–2258, Oct. 2007.
- [7] M. Lu, X. Meng, W. Yin, Z. Qu, F. Wu, J. Tang, H. Xu, R. Huang, Z. Chen, Q. Zhao, Z. Zhang, and A. Peyton, "Thickness measurement of non-magnetic steel plates using a novel planar triple-coil sensor," *NDT E Int.*, vol. 107, Oct. 2019, Art. no. 102148.
- [8] W. Yin, X. J. Hao, A. J. Peyton, M. Strangwood, and C. L. Davis, "Measurement of permeability and ferrite/austenite phase fraction using a multi-frequency electromagnetic sensor," *NDT E Int.*, vol. 42, no. 1, pp. 64–68, Jan. 2009.
- [9] I. D. Adewale and G. Y. Tian, "Decoupling the influence of permeability and conductivity in pulsed eddy-current measurements," *IEEE Trans. Magn.*, vol. 49, no. 3, pp. 1119–1127, Mar. 2013.
- [10] X. Ma and A. J. Peyton, "Eddy current measurement of the electrical conductivity and porosity of metal foams," *IEEE Trans. Instrum. Meas.*, vol. 55, no. 2, pp. 570–576, Apr. 2006.
- [11] X. Chen and Y. Lei, "Electrical conductivity measurement of ferromagnetic metallic materials using pulsed eddy current method," *NDT E Int.*, vol. 75, pp. 33–38, Oct. 2015.
- [12] W. Yin and K. Xu, "A novel triple-coil electromagnetic sensor for thickness measurement immune to lift-off variations," *IEEE Trans. Instrum. Meas.*, vol. 65, no. 1, pp. 164–169, Jan. 2016.
- [13] L. Shu, H. Songling, and Z. Wei, "Development of differential probes in pulsed eddy current testing for noise suppression," *Sens. Actuators A, Phys.*, vol. 135, no. 2, pp. 675–679, Apr. 2007.
- [14] H. Hoshikawa, K. Koyama, and H. Karasawa, "A new eddy current surface probe without lift-off noise," *AIP Conf. Proc.*, vol. 557, no. 1, pp. 969–976, Jan. 2001.
- [15] C. Wang, M. Fan, B. Cao, B. Ye, and W. Li, "Novel noncontact eddy current measurement of electrical conductivity," *IEEE Sensors J.*, vol. 18, no. 22, pp. 9352–9359, Nov. 2018.
- [16] D. Wen, M. Fan, B. Cao, B. Ye, and G. Tian, "Extraction of LOI features from spectral pulsed eddy current signals for evaluation of ferromagnetic samples," *IEEE Sensors J.*, vol. 19, no. 1, pp. 189–195, Jan. 2019.
- [17] B. de Halleux, B. de Limburg Stirum, and A. Tchelintsev, "Eddy current measurement of the wall thickness and conductivity of circular non-magnetic conductive tubes," *NDT E Int.*, vol. 29, no. 2, pp. 103–109, Apr. 1996.
- [18] J. C. Moulder, E. Uzal, and J. H. Rose, "Thickness and conductivity of metallic layers from eddy current measurements," *Rev. Sci. Instrum.*, vol. 63, no. 6, pp. 3455–3465, Jun. 1992.
- [19] W. Yin, S. J. Dickinson, and A. J. Peyton, "Imaging the continuous conductivity profile within layered metal structures using inductance spectroscopy," *IEEE Sensors J.*, vol. 5, no. 2, pp. 161–166, Apr. 2005.
- [20] F. Loete, Y. Le Bihan, and D. Mencaraglia, "Novel wideband eddy current device for the conductivity measurement of semiconductors," *IEEE Sensors J.*, vol. 16, no. 11, pp. 4151–4152, Jun. 2016.
- [21] X. Ma, A. J. Peyton, and Y. Y. Zhao, "Eddy current measurements of electrical conductivity and magnetic permeability of porous metals," *NDT E Int.*, vol. 39, no. 7, pp. 562–568, Oct. 2006.
- [22] Y. Yu, Y. Zou, M. A. Hosani, and G. Tian, "Conductivity invariance phenomenon of eddy current NDT: Investigation, verification, and application," *IEEE Trans. Magn.*, vol. 53, no. 1, pp. 1–7, Jan. 2017.
- [23] Y. Yu, Y. Zou, M. Jiang, and D. Zhang, "Investigation on conductivity invariance in eddy current NDT and its application on magnetic permeability measurement," in *Proc. IEEE Far East NDT New Technol. Appl. Forum (FENDT)*, May 2015, pp. 257–262.
- [24] M. Lu, W. Zhu, L. Yin, A. J. Peyton, W. Yin, and Z. Qu, "Reducing the lift-off effect on permeability measurement for magnetic plates from multifrequency induction data," *IEEE Trans. Instrum. Meas.*, vol. 67, no. 1, pp. 167–174, Jan. 2018.
- [25] M. Lu, R. Huang, W. Yin, Q. Zhao, and A. Peyton, "Measurement of permeability for ferrous metallic plates using a novel lift-off compensation technique on phase signature," *IEEE Sensors J.*, vol. 19, no. 17, pp. 7440–7446, Sep. 2019.
- [26] G. Y. Tian and A. Sophian, "Reduction of lift-off effects for pulsed eddy current NDT," *NDT E Int.*, vol. 38, no. 4, pp. 319–324, Jun. 2005.

- [27] D. I. Ona, G. Y. Tian, R. Suthaweekul, and S. M. Naqvi, "Design and optimisation of mutual inductance based pulsed eddy current probe," *Measurement*, vol. 144, pp. 402–409, Oct. 2019.
- [28] M. Lu, H. Xu, W. Zhu, L. Yin, Q. Zhao, A. Peyton, and W. Yin, "Conductivity lift-off invariance and measurement of permeability for ferrite metallic plates," *NDT E Int.*, vol. 95, pp. 36–44, Apr. 2018.



ZHONGWEN JIN received the B.Sc. degree in measuring, metering technique, and instrument from Beihang University, China, in 2004, and the M.Sc. and Ph.D. degrees in electrical and electronics engineering from The University of Manchester, U.K., in 2006 and 2010, respectively. He was appointed as a part-time Professor with the Department of Electronics and Information Engineering, Hangzhou Dianzi University, China. He is currently a Senior Scientist and Principal Investigator with the Zhejiang Energy Group Research Institute, Hangzhou, China. His current research interests include instrumentation, applied sensor systems, electromagnetics, and microwave tomography systems.



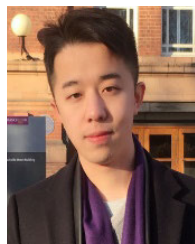
YUWEI MENG received the Ph.D. degree from the State Key Lab of CAD & CG, Zhejiang University, in 2012. He was appointed as a Research Assistant with The Hong Kong Polytechnic University, in 2008 and 2010, and The Chinese University of Hong Kong, in 2009. He is currently the Director of the Department of Industrial Informatization, Zhejiang Energy Group Research Institute, Hangzhou, China. His research interests include applied sensor systems, industrial big data analysis, and machine automation and optimization.



RONGDONG YU received the B.S. and Ph.D. degrees from the College of Computer, Zhejiang University, in 2004 and 2012, respectively. He is currently an Engineer with the Zhejiang Energy Group Research Institute, Hangzhou, China. His current research mainly involves industrial information, especially focuses on instrumentation, industrial big data analysis, and the information security of industrial control systems.



RUOCHEN HUANG is currently pursuing the Ph.D. degree with the School of Electrical and Electronics Engineering, The University of Manchester, under the supervision of W. Yin, mainly working on finite-element method (FEM) modeling software packages for electromagnetic (EM) simulations.



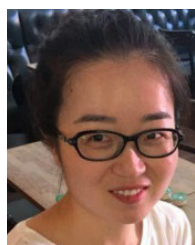
MINGYANG LU (Member, IEEE) received the B.S. and Ph.D. degrees from the School of Electrical and Electronics Engineering, The University of Manchester, U.K., in 2014 and 2018, respectively, under the supervision of W. Yin, mainly worked on developing a finite-element method (FEM) software to solve electromagnetic (EM) simulation considering random geometry and material properties, including microstructures. He is currently a Research Associate with The University of Manchester. He has authored or coauthored over 30 publications. His current research interests include modeling magnetic induction effects, finite-element method (FEM) modeling software packages on electromagnetic (EM) simulations, and the inversion of EM properties for metallic structures.



HANYANG XU received the B.Eng. and M.Sc. degrees in electrical and electronics engineering from The University of Manchester, in 2013 and 2014, respectively, where he is currently pursuing the Ph.D. degree in sensing and imaging. His current research mainly involves electromagnetic testing on welding inspection and imaging.



XIAOBAI MENG received the master's degree from The University of Manchester. She is currently pursuing the Ph.D. degree with the Faculty of Arts, Science, and Technology, The University of Northampton. Her current research interests include modeling magnetic induction effects, finite-element method (FEM) modeling software packages on electromagnetic (EM) simulations, and the inversion of EM properties for metallic structures.



QIAN ZHAO is currently a Professor with the College of Engineering, Qufu Normal University. She is mainly working on electromagnetism and electrical engineering.



ZHIJIE ZHANG is currently a Professor with the National Key Laboratory for Electronic Measurement Technology, North University of China. His research interests are thermocouple sensors, wireless sensors, Eddy current testing, and FPGA-based temperature measurements.



ANTHONY PEYTON received the B.Sc. degree in electrical engineering and electronics and the Ph.D. degree from The University of Manchester Institute of Science and Technology (UMIST), Manchester, U.K., in 1983 and 1986, respectively. He was a Principal Engineer with Kratos Analytical Ltd., Manchester, from 1986 to 1989, where he was involved in developing precision electronic instrumentation systems for magnetic sectors and quadrupole mass spectrometers. He joined the Process Tomography Group, UMIST, where he was a Lecturer. In 1996, he was a Senior Lecturer with Lancaster University, Lancaster, U.K., where he was a Reader in electronic instrumentation, in 2001, and a Professor, in 2004. Since 2004, he has been a Professor of electromagnetic tomography engineering with The University of Manchester, Manchester. His current research interests include instrumentation, applied sensor systems, and electromagnetics.



WULIANG YIN (Senior Member, IEEE) received the B.Sc. and the M.Sc. degrees in electronic measurement and instrumentation from Tianjin University, Tianjin, China, in 1992 and 1995, respectively, and the Ph.D. degree in automotive electronics from Tsinghua University, Beijing, China, in 1999. He was appointed as a Mettler Toledo (MT) Sponsored Lecturer with the Department of Electrical and Electronics Engineering, School of Engineering, The University of Manchester, Manchester, U.K., in 2012, and was promoted to a Senior Lecturer, in 2016. He has authored one book and more than 230 articles, and was granted more than ten patents in the areas of electromagnetic sensing and imaging. He was a recipient of the Science and Technology Award from the Chinese Ministry of Education, in 2000, and the Williams Award from the Institute of Materials, Minerals, and Mining, in 2014 and 2015.

• • •